The Spanish Review of Financial Economics

www.srfe.journals.es

HAZARDS MITIGATION OF LAHAR FLOWS ON SEMERU VOLCANO AFTER THE 4 DECEMBER 2021 ERUPTION BASED ON PS-INSAR

CHOLISINA ANIK PERWITA[a], FARIDHA APRILIA[a], SUKIR MARYANTO[a], HARUN ARRASYID[a], AND AQYLA FARAHTSABITAH[a]

[a]Geophysical Engineering Study Program, Department of Physics, Faculty of Mathematics and Natural Sciences, Brawijaya University. Jl. Veteran Ketawanggede, Lowokwaru, Malang City 65145, Indonesia.

Abstract

Volcanic eruption is one of the phenomena that can change the volcanic landscape drastically. Monitoring of volcanic edifices after eruptions should be considered to further understand the potential hazards in the future. Satellite monitoring is a reliable technique for assessing deformation in a volcano. InSAR was applied to detect material build-up after the eruption phase of Semeru Volcano in December 2022. As a consequence of the opening crater along with the InSAR result, a lahar product after the eruption was deposited in the southwest direction. Significant deformations were indicated by PS-InSAR near the crater, which was characterized by a LOS displacement of -10 to -40 mm/year, indicating scouring of the pyroclastic material moving down the slope. The accumulation of pyroclastic flows from the abrading process below was detected in the proximal zone of Semeru, as shown by the positive LOS displacement ranging from 10 to 40 mm/year. The field survey conforms to the PS InSAR results, where unconsolidated material, ranging in size from gravel to boulders, piles up approximately 4-5 m in Curah Kobokan. Highly unconsolidated material tends to move easily by water and threaten the surrounding settlements. Overlying PS InSAR and drainage pattern in the flank of Semeru, concluding several locations that have a high-risk potential of being affected by lahar flows are Curah Kobokan, Supiturang Village, Pronojiwo District, then Tulungrejo, Pasropan Village, Pasrujambe District, Lumajang Regency.

Keywords: Deformation, Semeru, PS InSAR, lahar flow.

INTRODUCTION

Lahar is a hazardous volcanic phenomenon that is found in many volcanoes. Lahar is a term adapted from the Indonesian language that refers to a fast-moving material that combines water and sediment, making it a big power to destroy. Except for volcanic ashfall and pyroclastic flow, lahars should be considered the main threat, especially in volcanoes located in tropical countries that have a large range or rainy seasons. The fatalities linked to volcanic eruptions worldwide were 40% during the 20th century (Dumaisnil et al., 2010; Vallance, 2000). The vast amount of pyroclastic deposits that cover the volcanic cone on the flanks of Mt. Semeru (3676 m) in East Java creates suitable conditions for lahar formation. The erosion rate of Mt. Semeru is 4 km^2/year, which is comparable to that of other explosive volcanoes in humid climates (Thouret et al. 2007). Furthermore, because of the ongoing sediment turnover, Mount Semeru is one of the world's major generators of lahars (Thouret et al., 2007). Compared to Merapi, which has almost similar rainfall frequency and intensity, lahars in Semeru occur more frequently for several reasons; for example, Semeru has a steeper slope than Merapi (about 33 °), and Vulcanian explosions in Semeru provide a more continuous and voluminous sediment supply (Lavigne, 2004). Semeru has been erupting constantly since 1967, with vulcanian explosions lasting 10 minutes to 1 hour and ash plumes rising 300-1000 meters above the active crater. During periods of increased volcanic

activity, gravity- driven dome-collapse pyroclastic flows and more mobile scoria flows moved as far as 115 km from the vent in radial troughs that drained the south and southeast sides, as seen in 1994, 1995, and 2002. In the case of the Semeru eruption in 2021, eruptive activity was preceded by heavy rainfall, causing pyroclastic flows to mix with rainwater and form debris flow or "lahar." Research by the Earth Observatory of Singapore - Remote Sensing Lab (EOS-RS) shows that the area on the surface hit by pyroclastic flows and lahars in the southeastern sector of Semeru reaches Curah Kobokan. Compared to the eruption in 2020, the eruption on December 4, 2021, is classified as a fairly large eruption, even though it has almost the same hot cloud glide distance of 11 km. Satellite monitoring of volcanic ash in Darwin (Darwin Volcanic Ash Advisory Centre, VAAC Darwin) recorded that the eruption column reached 15 km above sea level at 4:30 PM (Sennert, 2021). The changing volcanic edivice after eruption and accumulation of the deposit area near the flank should be monitored over time as a mitigation plan. In most cases, edifice instability develops as a result of one or more of several causes such as magma emplacement, slope overloading or oversteepening, and peripheral erosion. Understanding the possible size of structural collapses and the related eruptive activity has significant consequences for the development of monitoring and hazard mitigation techniques for vulnerable volcanoes, which must now account for the probability of future collapse events (McGuire, 1996). Since 1980, Interferometry Synthetic Aperture Radar (InSAR) has been widely used to monitor earth deformations such as earthquakes (Massonnet et al., 1993), movement of permafrost (Goldstein, et al., 1993), volcanoes (Massonnet, et al., 1995), landslides (Amelung, et al., 1999), and underground water flows. In volcano monitoring, the practical application of lithological and geomorphological changes to the Earth's surface in damage assessment and disaster monitoring is crucial (Wadge et al., 2002; Stramondo et al., 2006; Saepuloh et al., 2010; Bignami et al., 2013; Solikhin et al., 2015). Here, we present our new results from PS-InSAR of surface deformation after the eruption of 2021. The highest deformation rate was sampled from the upslope and downslope, and its changes due to the eruption were investigated. High deformation is assumed to be the most rapid sedimentation in catchments, and field observations are used to validate the data to gain information related to the sediment package. Finally, we propose a possible hazard-related lahar that may occur as a consequence of unconsolidated sedimentation material.

METHODS

The data required for PS-InSAR processing is Sentinel-1 Single Look Complex (SLC) data, DEM data, and orbital data, which can be downloaded free of charge from https://vertex.daac.asf.alaska.edu/. The satellite data range of 18 data starts from January 2021 to June 2022, with one data selected as master, namely November 2021, and the other data as slaves. All these data come from the Sentinel-1A satellite with ascending orientation (south- north), which has a wavelength of 0.56 cm or is classified as C-band type and polarization in the form of VV and has a resolution of 5 × 20 m because it is an interferometric wide swath mode (Flores et al., 2019). The calculation of the coregistration and interferogram produces coregistration data, which is a match between two images, and an interferogram that contains the phase difference between the master and slave. The phase difference in question is the phase difference between the emitted wave and the reflected wave which describes the delay time between the two waves (Ferreti et al, 2007). Phase difference from one pair wave can be used to calculate the difference of acquisition object

by using the equation (1) below:

$$\emptyset_2 - \emptyset_1 = \frac{2\pi}{\lambda} 2R = \frac{4\pi}{\lambda}(R_2 - R_1) \qquad (1)$$

where Ø is the phase difference for each interferogram, λ is the wavelength, and R is the distance between the acquisition objects. In addition to the surface deformation components, the interferogram (ϕLOS) phase also contains other components, namely Δϕgeom, which is related to the difference in the geometry of the satellite's view, phase difference from the topography Δϕtopo, and phase difference from the atmospheric refraction
Δϕatm. As described in Equation (2),

$$\{\phi LOS\} = \Delta\phi def + \Delta\phi geom + \Delta\phi topo + \Delta\phi atm + \phi error \quad (2)$$

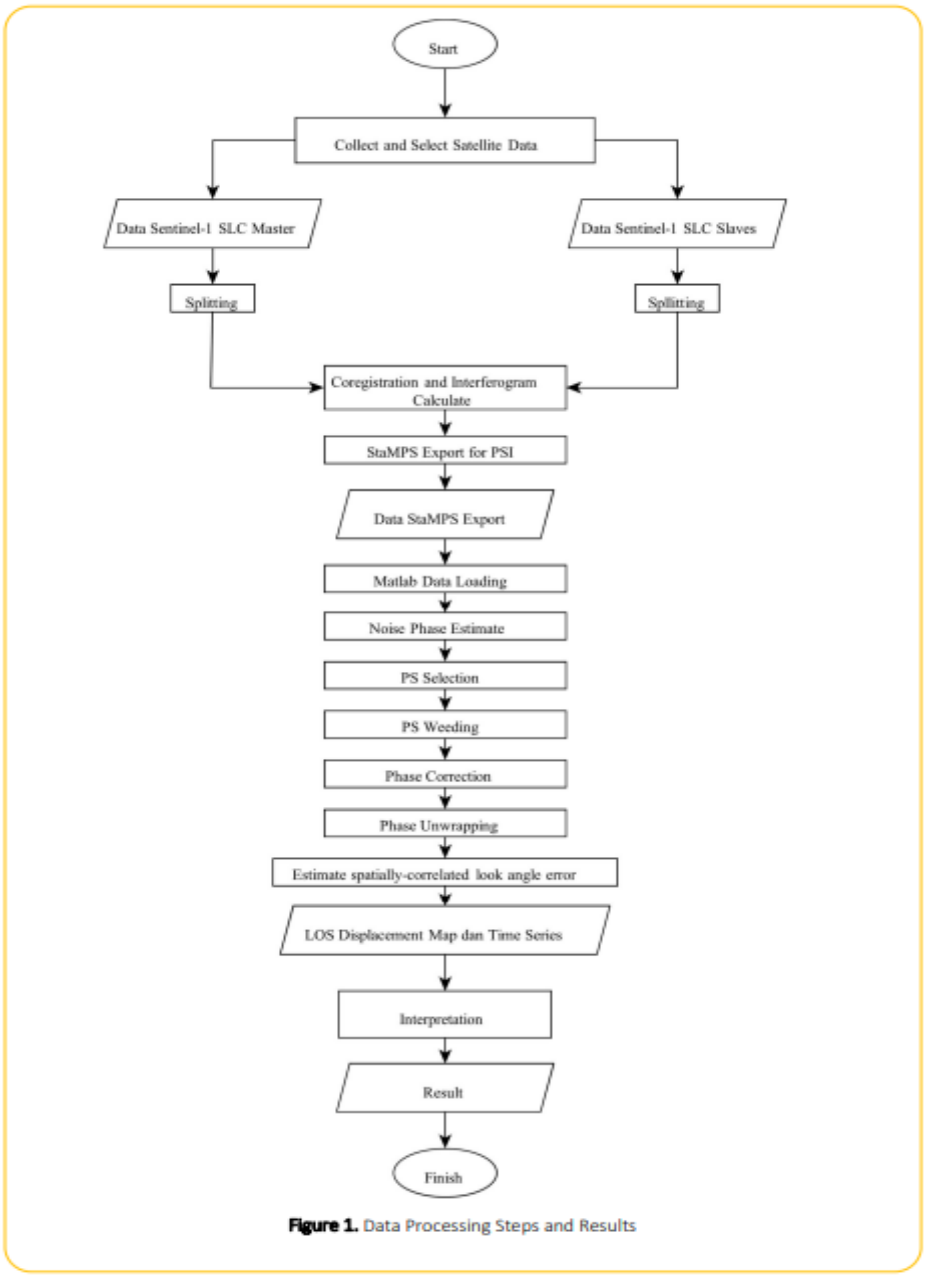

Figure 1. Data Processing Steps and Results

The geometry factor is solved by applying the exact orbit and estimating the perpendicular baseline between satellite orbits. This effect was eliminated by assuming ellipsoidal smooth earth. Errors in predictable satellite orbits due to solar radiation pressure. DEM was used in processing to eliminate the phases introduced by the topography. The largest source of phase error was caused by variations in atmospheric refraction between $\Delta\phi$atm acquisitions. The ϕ error is an additional noise that describes the phase noise caused by scattering and heat noise from instruments (Parker, 2017).

The results of coregistration and interferogram were exported so that they could be further processed using the Stanford Method for Persistent Scatterers (StaMPS) method with MATLAB software. StaMPS is a PS-InSAR processing method that uses a set of C++-based software and Matlab scripts regularly according to the Hooper et al. (2012) algorithm, which was developed so that it can be used even if applied in terrain without man-made structures or irregular deformations (Hooper et al., 2018).

The StaMPS used in this study consists of seven stages. The first stage is data loading, which is used to input the coregistration and interferogram data in the format and location corresponding to the StaMPS algorithm. Phase noise value estimation of each pixel candidate of each interferogram was performed based on several parameters, including maximum topographic error, pixel size, the weighting of each pixel, filter combined low-pass, adaptive phase, and the maximum number of iterations (Hooper et al., 2010). The third step in stamps is the PS selection process, which is selected based on the phase-noise criteria in the previous stage. This stage also estimates the percentage density of other pixels (non-PS). The fourth step is the PS weeding stage, which sorts and eliminates pixels that are not selected. Next, phase correction corrects the phase of spatially correlated pixels. Sixth-stage stamps for converting interferograms that are unitary $-\pi$ to π are converted into absolute phases of integer multiplier 2π, because they are more related to topography and deformation. Phase variation between two points on a flattened interferogram provides a measurement of the actual height variation, having removed all integers from the height (Ferreti et al, 2007). Next, the estimated stage spatially correlates the look angle error to calculate the error look angle that has been correlated in stages three and five. From the processing of stamps 1-7, a map of the distribution of LOS over time was obtained. Based on the results of the data processing, interpretation and mitigation were carried out by considering geological data. The entire data-processing stage is shown in Figure 1.

RESULTS

The results of Sentinel satellite image data processing using the PS-InSAR method are shown in Figure 2. The range of data used in this study was from January 2021 to June 2022, covering the Mount Semeru area. The selection of the data range was based on the last eruption of Mt. Semeru, which occurred on December 4, 2021. Data before and after the eruption were used to observe the deformation that occurred.

The deformation that occurs in the body of Mount Semeru based on the results of processing using the PS-InSAR method shows that the speed of deformation that occurs at the location of this study is indicated by the LOS displacement value ranging from -40 mm/year to 40 mm/year. From the figure, it can be seen that the North, West, and South areas are relatively not deformed. The eastern area shows little deformation as indicated by the yellow to light

green PS-InSAR points, which reveals that the LOS displacement rate ranges from 0 to -10 mm/year. The area in the southeastern part shows significant deformation, as indicated by the dark red to dark blue PS-InSAR points with LOS displacement values ranging from -40 mm/year to 40 mm/year. The results of this study correspond with the eruption that occurred on December 4, 2021, where the crater opening and pyroclastic material flowed southeast. The Southeast area is the focus of the discussion of the results of this study.

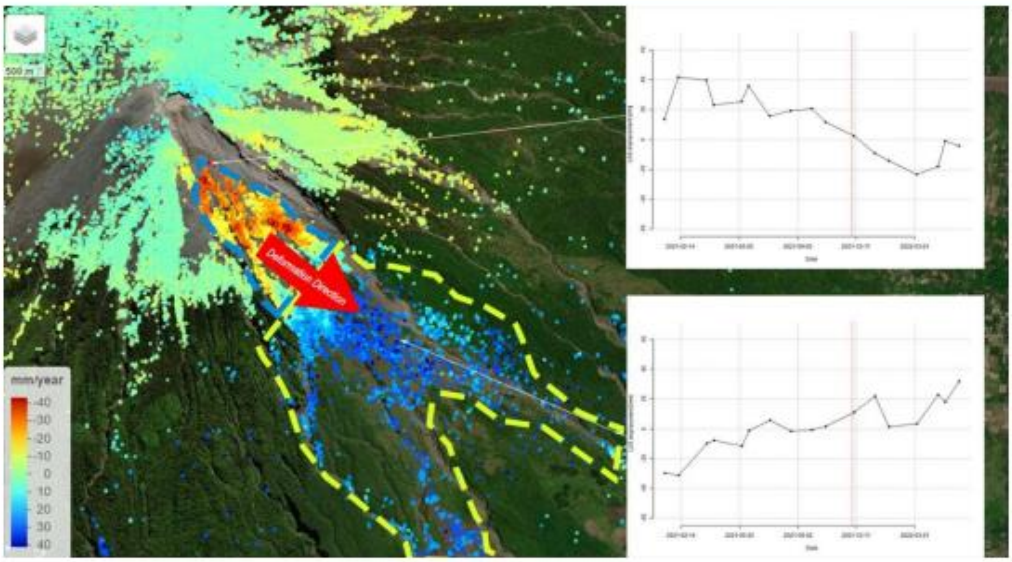

Figure 2. Mount Semeru deformation based on PS InSAR (Sentinel Image January 2021 to June 2022).

Significant Deformation in the Southeast Area

The zones with significant deformation in the southeast can be grouped into two categories. The first category is the zone with yellow to dark red PS-InSAR dots that are relatively close to the center of the Semeru eruption. The zone is characterized by a LOS displacement of -10 mm/year to -40 mm/year, which indicates an area that is experiencing negative deformation or a decrease in ground elevation. The general pattern of negative deformation at this location is interpreted as a result of the scouring of the body of the volcano, which occurred as a result of the eruption in December 2021.

This condition can be observed from the graph of the deformation that occurred during the time period of the data used (Figure 3). From the graph, it can be seen that from January to March 2021, there was a positive deformation, which was expected to occur due to the buildup of pyroclastic material resulting from previous small eruptions. From March to July 2021, there was a decrease followed by relatively constant ground surface conditions or no deformation until early December 2021. After that, there was a significant negative deformation from December 2021 to February 2022, which was interpreted to have occurred due to the scouring of pyroclastic material moving down the slope during the eruption on December 4, 2021. In March 2022, the positive deformation that occurred was possible due to the accumulation of material from lahar flows that carried pyroclastic material to the distal zone of the volcano.

The zone with the general pattern of positive deformation is in the lower southeastern part

of Semeru's body. This zone is indicated by the distribution of Ps-InSAR points in light blue to dark blue, which show LOS displacement values ranging from 10 mm/year to 40 mm/year. From Figure 2, it can be seen that the closer to the distal zone in the southeast of the Semeru Volcano, the greater the LOS displacement, as indicated by the color of the PS In-SAR points from blue to dark blue. The deformation graph is shown in detail in Figure 4. From the graph, it can be observed that from January 2021 to January 2022, it is estimated that positive deformation occurred due to the accumulation of material carried by the lahar flow. This deformation occurred significantly during the rainy season (January – May 2021). After the eruption from January to February 2022, there was a significant negative deformation, which was possible because of the scour of the lahar flow materials. The lahar flow was estimated to be larger than before, with a wider range, and this area is an area of erosion (scour), whereas it was previously an area of sedimentation. From March to June 2022, there was another sedimentation of material brought by lahar flows from the eruption of Semeru Volcano with smaller intensity.. Field Observation

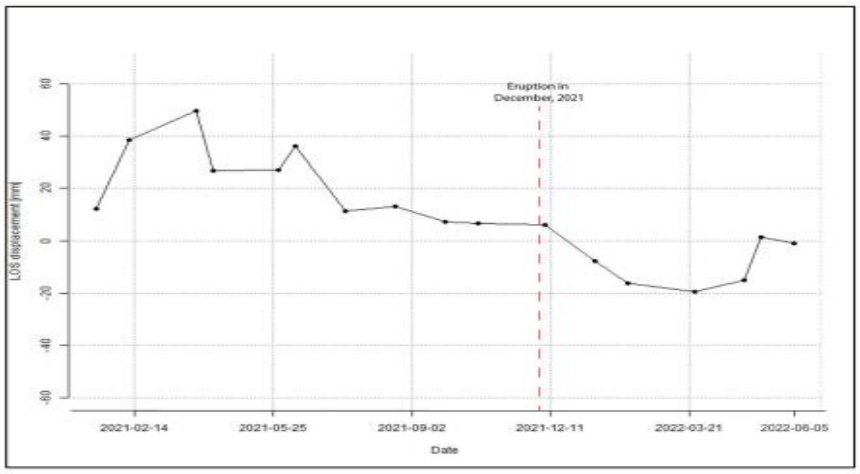

Figure 3. Time series graph of the negative deformation zone

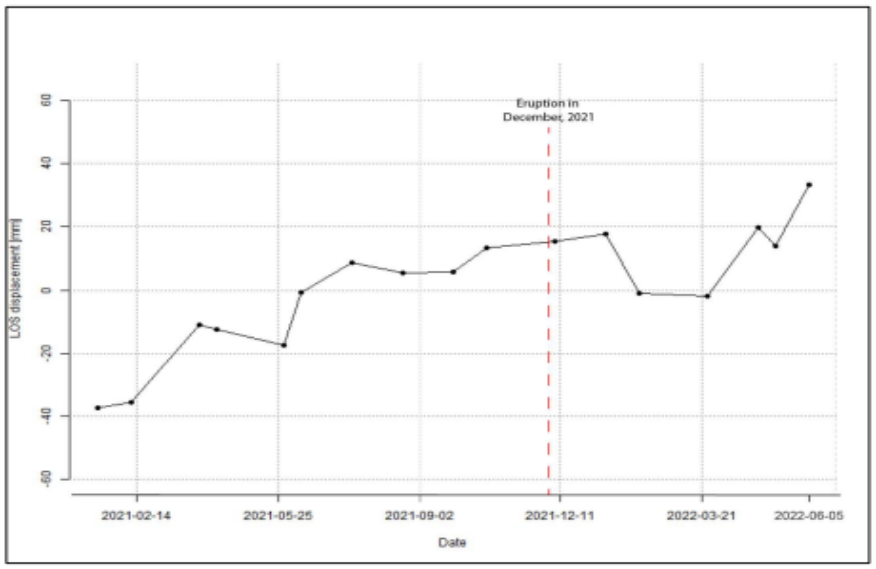

Figure 4. Time series graph of the positive deformation zone

A field survey was conducted to identify material characteristics in the positive-deformation zone. The survey was located in Kali Besuk Semut, Curah Kobokan, Supiturang Village, Pronojiwo District, Lumajang Regency. From the field survey, it can be observed that the location is composed of pyroclastic material and lahar deposits. The thickness of the new material as a product of the last eruption in December 2021, was approximately 4-5 m (Figure 5). The materials are unconsolidated, poorly sorted, open fabric, with andesite rock fragments ranging in size from gravel to boulders (diameter up to 1.5 m), while the matrix is composed predominantly of sand-to- gravel-sized materials (< 4 mm). Unconsolidated materials have the potential to produce lahar flows when mixed with water (Parfitt and Wilson, 2008).

Figure 5. Lahar and pyroclastic deposit products in the positive deformation zone

DISCUSSION

Mitigation of Potential Lahar Flow Hazard Zones

Lahar or debris flows consist of a mixture of water and solids that move toward a lower area. In volcanic areas, the solid material that makes up the lahar is generally composed of material from a volcanic eruption. According to Parfitt and Wilson (2008), lahars are a long-term threat after a volcanic eruption, especially if the material resulting from the eruption is dominated by unconsolidated material. The materials easily mix with water and become a lahar flow. In Semeru, lahar flows are often triggered by rain, which causes runoff to mix with unconsolidated pyroclastic material moving along the river channels. Therefore, the amount of material accumulated and the distance to the river flow were used as parameters to determine the potential hazard zone against lahars in this study.

PS-InSAR deformation data overlaid with a map of the drainage pattern and the existence of residential areas were used to mitigate the potential hazards of lahars. Based on these considerations, the locations that have a high-risk potential of being affected by lahar flows are Curah Kobokan, Supiturang Village, Pronojiwo District, and Tulungrejo, Pasropan Village, Pasrujambe District, Lumajang Regency. The area marked with a yellow circle in Figure 6 is located around the river, where there is a large accumulation of pyroclastic material upstream, based on the results of the PS-InSAR deformation processing. The results of this study are expected to be considered by authorities when handling potential lahar flows around Semeru Volcano.

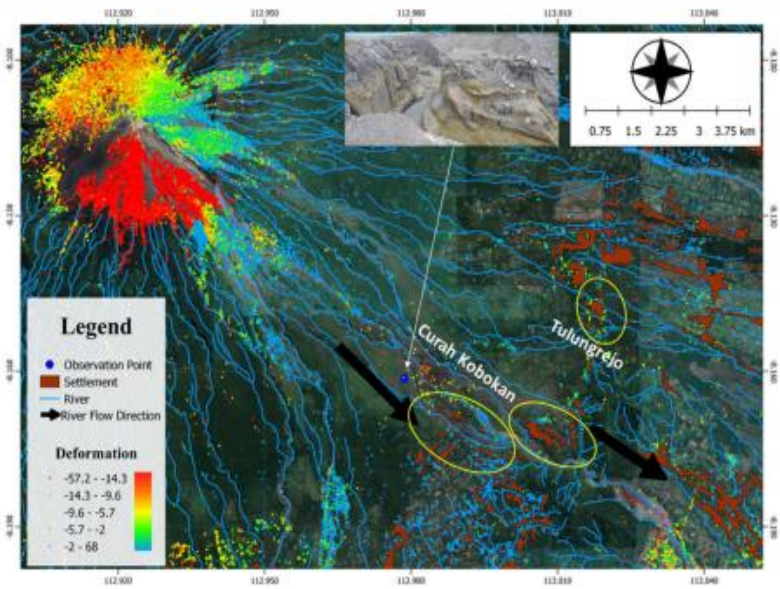

Figure 6. Mitigation of potential hazard zones of Semeru lahar flows.

CONCLUSIONS

Based on this research, it can be concluded that the zone of significant deformation was located in the direction of the opening of the Semeru eruption (southeast). The area with negative deformation was closer to the peak indicated by the LOS displacement from -10 mm/y to -40 mm/y. This was probably caused by the scoured material coming out of the crater. This material then accumulates in the zone of positive deformation located in the

downstream area, which is indicated by the LOS displacement from 10 to 40 mm/y. An area with positive deformation was located downstream. The deformation appears significant, especially after the eruption on December 4, 2021. Areas with high potential to be affected by debris flow (lahar) are Curah Kobokan, Supiturang Village, Pronojiwo District, then Tulungrejo, Pasropan Village, Pasrujambe District, Lumajang Regency.

ACKNOWLEDGMENTS

The authors acknowledge the Institute for Research and Community Service (LPPM), Brawijaya University, which funded this research through the Hibah Peneliti Pemula (HPP) in 2022.

References

1. Amelung , F., Galloway , D. L., Bell, J. W., Zebker, H. A., & Laczniak, R. J. (1999). Sensing the ups and downs of Las Vegas: InSAR reveals structural control of land subsidence and aquifer-system deformation. Geology, 27(6), 483–486. https://doi.org/10.1130/0091-7613(1999)027%3C0483:STUADO%3E2.3.CO;2
2. Dusmaisnil , C., Thouret , J.-C., Chambon , G., Doyle , E., Cronin, S., & Surono. (2010). Hydraulic, physical and rheological characteristics of rain-trigerred lahars at Semeru volcano, Indonesia. Earth Surface Processesand Landforms(35), 1573-1590
3. Goldstein, R. M., Engelhardt, H., Kamp B, & Frolich, R. M. (1993). Satellite radar interferometry for monitoring ice sheet motion: application to an antarctic ice stream. Science, 262, 1525–1530. https://doi.org/10.1126/science.262.5139.1525
4. Hooper, A., Spaans, K., Bekaert, D., Cuenca, M. C., Arıkan, M., & Oyen, A. (2018). StaMPS/MTI manual. Delft Institute of Earth Observation and Space Systems Delft University of Technology, Kluyverweg, 1, 2629.
5. Hooper, A., Bekaert, D., Spaans, K., & Arıkan, M. (2012). Recent advances in SAR interferometry time seriesanalysis for measuring crustal deformation. Tectonophysics, 514, 1-13.
6. Ferretti, Alessandro Monti-Guarnieri, Andrea Virgilio Prati, Claudio Maria Rocca, Fabio D. Massonnet. (2007).
7. INSAR Principles B. Politecnico Di Milano. http://hdl.handle.net/11311/550055
8. Flores, A., Herndon, K., Thapa, R., & Cherrington, E. (2019). The SAR Handbook: Comprehensive Methodologies for Forest Monitoring and Biomass Estimation. https://doi.org/10.25966/nr2c-s697
9. Lavigne, F. (2004). Rate of Sediment Yield Following Small-Scale Volcanic Eruption : A Quantitative Assessment at the Merapi and Semeru Stratovolcanoes, Java, Indonesia . Earth Survace Processes and Landform, 29, 1045- 1058.
10. McGuire, W., Jones, A., & Neuberg, J. (1996). Volcano Instability on the Earth and Other Planets. Geological Society Special Publication No.10, 1-23.
11. Massonnet , D., Rossi, M., Carmona, C., Adagna, F., Peltzer, G., Feigl K, & Rabaute T. (1993). The displacement field of the Landers earthquake mapped by radar interferometry. Nature, 8(364), 138–142. https://www.nature.com/articles/364138a0
12. Massonnet, D., Briole, P., & Arnaud , A. (1995). Deflation of Mount Etna monitored by spaceborne radar interferometry. Nature, 375, 567–570. https://www.nature.com/articles/375567a0
13. Parfitt, E. A., & Wilson, L. (2008). Fundamentals of Physical Volcanology, 1st Edition. Blackwell Publishing
14. Parker, A.L. (2017). Systematic assessment of atmospheric uncertainties for InSAR data at volcanic arcs using large-scale atmospheric models: Application to the Cascade Volcanoes. Springer, pp 59–90

15. Saepuloh, A., Koike, K., Omura, M., Iguchi, M., & Setiawan, A. (2010). SAR-and gravity change-based characterization of the distribution pattern of pyroclastic flow deposits at Mt. Merapi during the past 10 years. Bull. Volcanol., 72(2), 221–232.

16. Sennert, K. D. (2021). Report on Semeru (Indonesia) In: Senner, S K (ed.), Weekly Volcanic Activity Report, 1 December - 7December 2021. Institution and US Geological Survey. Smithsonian

17. Solikhin, A., Pinel , A., Vandemeulebrouck, J., Thouret, J., & Hendrasto , M. (2015). Mapping the 2010 Merapi pyroclastic deposits using dual-polarization Synthetic Aperture Radar (SAR) data. Remote Sens. Environ, 158, 180–192.

18. Stramondo, S., Bignami, C., Chini, M., Pierdicca, N., & Tertulliani, A. (2006). Satellite radar and optical remote sensing for earthquake damage detection: results from different case studies. Int. J. Remote Sens., 27(20), 4433–4447.

19. Thouret , J.-C., Lavigne , F., Suwa , H., Sukatja , B., & Surono. (2007). Volcanic hazards at Mount Semeru, East Java(Indonesia), with emphasis on lahars. Bulletin of Volcanology, 7(2), 221-244.

20. Valance, J. (2000). Lahars. In H. Sigurdsson (Ed.), Encyclopedia of Volcanoes (pp. 601–616). San Diego: Academic Press.

21. Wadge, G., Scheuchl, B., & Stevens, N. (2002). Spaceborne radar measurements of the eruption of Soufriere Hills volcano, Montserrat. Geological Society, London, Memoirs, 21(1), 583-594.